JCTC Journal of Chemical Theory and Computation

Article

pubs.acs.org/JCTC

A Configuration Interaction Picture for a Molecular Environment Using Localized Molecular Orbitals: The Excited States of Retinal Proteins

Jun-ya Hasegawa,*[,†,‡,∥,⊥] Kazuhiro J. Fujimoto,[§] and Tsutomu Kawatsu[†,∥]

[†]Fukui Institute for Fundamental Chemistry, Kyoto University, 34-4 Takano-Nishihiraki-cho, Sakyo-ku, Kyoto 606-8103, Japan

[‡]Quantum Chemistry Research Institute, Kyodai Katsura Venture Plaza, Goryou Oohara 1-36, Nishikyo-ku, Kyoto 615-8245, Japan

[§]Department of Computational Science, Graduate School of System Informatics, Kobe University, 1-1, Rokkodai, Nada, Kobe 657-8501, Japan

[∥]Institute for Molecular Science, National Institute of Natural Science, 38 Nishigo-Naka, Myodaiji, Okazaki 444-8585, Japan

Supporting Information

ABSTRACT: Electronic excitations of chromophores in proteins and solutions are associated with the electronic response of the molecular environment. The underlying interactions are important origins of solvatochromism. We performed large-scale configuration interaction singles (CIS) calculations (up to 1000 atoms) for retinal chromophores in proteins and methanol solution, in which one-electron processes (polarization and charge-transfer effects of the environment) are included. The present approach also improved the electrostatic potential, as compared to that described by a molecular mechanics (MM) force field. The CIS results were combined with the symmetry adapted cluster (SAC)-CI result using our own N-layer integrated molecular orbital molecular mechanics (ONIOM) method. As compared to the MM description, the CIS reduces the calculated excitation energy by 0.1−0.3 eV and also improves the relative excitation energies among retinal proteins. We applied our localized molecular orbital (LMO) transformation scheme to analyze the CI wave functions. The result clarified the contributions of the amino acids. In bacteriorhodopsin, Tyr185 contributes intermolecular CT excitations. The radial distribution of amino acids' contributions to the CI wave function was also analyzed. The results of the analysis are useful not only for understanding the molecular interactions and the role of amino acids in color tuning, but also for providing insight into the structure of the excited-state wave function for the molecular environment. An excitation-energy decomposition analysis also supported the results of the excited-state wave functions.

1. INTRODUCTION

The photoabsorption energy of a molecule depends on its surrounding environment, as in solvatochromism in organic molecules.[1] Depending on molecular interactions with the environment, the absorption energies of solvatochromic molecules vary significantly. In biological systems, the absorption energy of a retinal Schiff base (SB) depends on the surrounding environment,[2,3] a situation referred to as an opsin shift.[4] The absorption energy of a retinal deprotonated Schiff base (DPSB) is 3.4 eV in methanol (MeOH) solution,[5] while the absorption energy becomes 3.0 eV in a bacteriorhodopsin (bR) environment.[2,5] The retinal SB shows bathochromic variation over a wide energy range when the chromophore is protonated. In visual pigments, the absorption energies of the retinal protonated Schiff base are 2.99,[6] 2.33,[7] and 2.20 eV[7] in human blue (HB), green (HG), and red (HR) cone pigments, respectively.

To understand the reason for the variation in the absorption energy, many theoretical studies have been carried out (see refs 8−16 and references therein). One of the most popular ways to take into account of the environmental effect is a QM/molecular mechanics (MM)[17]-type approach in which the electrostatic potential (ESP) of amino acids is described by atom-centered point charges adopted in the MM force field.[18] The charges were derived from the ESP calculated using ab initio quantum chemical calculations.[18] These QM/MM studies clarify the important role of the ESP in the color tuning of retinal PSB. An important feature in the spectral shift is the synergy between the intramolecular charge transfer (CT) character during the transition and the ESP at the chromophore binding site produced by the protein environment.[11,12,19]

However, in our previous study on the opsin shift of DPSB,[20] the ES interaction provided only a negligible shift in the calculated excitation energies because of the small intramolecular charge-transfer (CT) character during the transition of DPSB. On the other hand, the absorption energies decreased by up to 0.25 eV when the MM force field was replaced by the CIS wave functions.[20] Because the QM contribution explained more than 25% of the total shift, we recognized that the QM effects and the QM-described ESP introduced by the CIS calculations are not negligible when investigating the origin of solvatochromism in protein environments. In our study on fluorescent protein,[21] the calculated fluorescent energy became more reliable when the environmental effect was described using CIS wave functions.

In previous studies, the electronic polarization effect of protein environments was investigated by means of a polarizable dielectric model,[22,23] frozen-density embedding,[24,25] an empirical polarization model,[26] and a QM/QM/MM model.[16] These

Received: June 19, 2012
Published: October 8, 2012

studies, however, did not consider orbital interactions between the retinal and its protein environment. A semiempirical CI calculation was also performed for bR and sRII[27] in which amino acid residues in the first solvation layer (FSL) were included in the QM region. This calculation considered orbital interactions at the SCF level. However, the protein's polarization effect was not included because the active orbitals in the CI calculation included only the π orbitals of the chromophore. Very recently, time-dependent density functional theory (TDDFT) and algebraic diagrammatic construction through second-order (ADC(2)) results for bluecone and rhodpsin were published.[28] The computational models was not enough large to investigate both polarization and CT effects. Under these circumstances, it was necessary to investigate both the orbital interactions and the polarization effects in a single excited-state calculation.

With the inclusion of these environmental QM effects, the origin of the QM effect should be investigated. Our interest is in identifying which amino acids provide contributions and what type of physical interaction is actually important. For this purpose, ordinary canonical molecular orbitals (CMOs) are not useful for the interpretation because the CMOs describing the environment are often delocalized. In addition, the delocalized MO picture introduces artificial configuration mixing, which modifies the orbital picture for the excited state.[29] We applied our hybrid MO localization scheme,[29] and delocalized CMOs were localized into each amino acid moiety. Consequently, excited configurations have clear physical meanings, such as local excitations in the amino acids and CTs between retinal chromophores and amino acids.

In this Article, we first explain the computational details of our investigation, including the performance of the MO localization scheme in section 2. In section 3.1, we summarize the results of large-scale SAC-CI:CIS/AMBER99 calculations for retinal proteins (HB, HG, HR, Rh, sRII, bR (BR state), and bR (M state)) and DPSB in MeOH solution, including the effects of the surrounding environment, incorporated into quantum chemical calculations to illustrate how the calculated excitation energy varied when the fixed point-charge model was replaced by wave functions. We then introduce an LMO picture to understand the calculated environmental QM effect (section 3.2). We further analyzed the environmental CI wave functions from a coarse-grained point of view to investigate the role of amino acids (section 3.3). Our conclusions are presented in section 4.

2. COMPUTATIONAL DETAILS

2.1. QM/MM Calculations. Atomic coordinates were obtained in our previous study[11,19,20] and optimized using the QM/MM method.[17,30] For DPSB in methanol solution, only DPSB was included in the QM region.[20] Methanol molecules belonged to the MM region. To obtain the initial structures for the QM/MM optimization, classical molecular dynamics calculations were performed using the AMBER 10 program,[31] and four snapshot structures were taken from the trajectory.[20] For PSBs in bR (BR state), sRII, and Rh and for DPSB in bR (M state), X-ray structures were adopted for the initial structures.[19,20] For HB, HG, and HR, the computationally determined structures[32] were modified before the QM/MM optimization.[11] In the QM/MM optimization, B3LYP/6-31G* and AMBER99[18] were employed for the electronic structure method and the classical force field, respectively. For the methanol case, the atomic coordinates of the MM atoms were frozen during the QM/MM optimization to retain the solvation structures.

To calculate the excitation energy, we gradually increased the size of the QM region. We used a computational model called the x Å model (x = 3, 4, 5, 6, etc.). In addition to the retinal chromophore, selected amino acids with shortest distances of less than x Å from the chromophore were included, where "x" was the effective radius of the QM region (r_{QM}) that was used as a threshold for selecting amino acids (see Figure 1b). A large

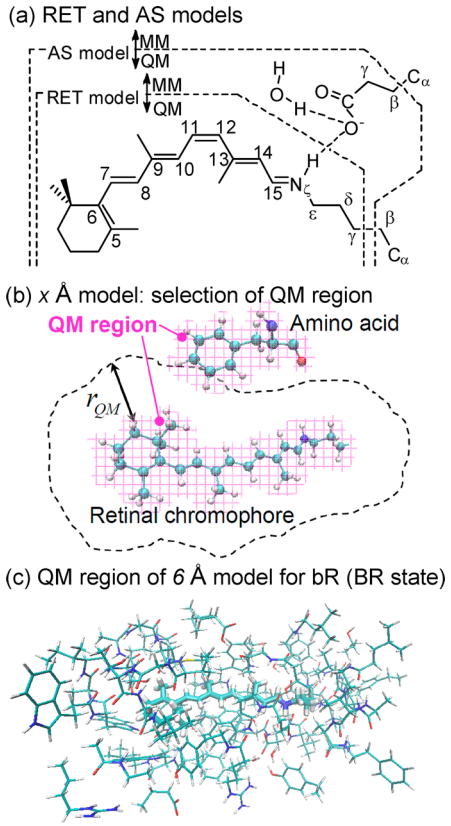

Figure 1. Computational models of (a) RET and AS models and (b) x Å model. (c) An example of the QM region (6 Å model for bR).

number of QM−MM borders existed in the x Å models. If two sequential amino acids were selected for the QM region, the peptide bond connecting the two amino acids was included in the QM region. If a neighboring amino acid was not selected for the QM region, the −CO− or −NH− unit in the peptide bond was replaced by a linking atom. A hydrogen atom as a link atom was placed on the C_α−C or C_α−N line with a Cα−H bond length of 1.09 Å. If only one Cys in a Cys−Cys bond was involved in the QM region, both Cys's were included in the QM region. In Figure 1c, we show an example of the QM region for the 6 Å model of bR (BR state). Regarding the MM region, the MeOH solution model considered solvent molecules up to 20 Å from the chromophore. In the protein cases, the rest of the atoms outside the QM region were included in the MM region. We also used the RET and AS models.[19,20] The RET model included only the retinal chromophore in the QM region. The "AS" model additionally included a counterion and a water molecule interacting with glutamate (see Figure 1a). A QM−MM border in the lysine residue connected to the retinal was placed at the C_β−C_γ bond (see Figure 1a). As a link atom, a hydrogen atom replaced the C_β atom and was placed on the C_β−C_γ line with a Cγ−H bond length of 1.09 Å. The charge of the replaced C_β atom was zeroed. Because of the QM−MM border, the total atomic charge of the lysine in the MM region

dx.doi.org/10.1021/ct300510b | J. Chem. Theory Comput. 2012, 8, 4452−4461

was not exactly zero. Additional MM charges were redistributed for this lysine, and the total charge was set to zero using a previously proposed scheme.[33] The counterion in the AS model also possesses a QM–MM border at the C_α–C_β bond. The procedure used to handle the QM–MM border was the same as that used for the lysine case.

To calculate the excited states with the x Å models, CIS/AMBER99 calculations were performed. The basis sets used were 6-31G* sets[34,35] for the retinal chromophore and 6-31G sets for the environment. Basis-sets' dependence was checked by extending the basis sets to 6-311+G* and 6-31G* sets for the retinal chromophore and the rest, respectively. As shown in Table S1 in the Supporting Information, the extension of the basis sets reduced the calculated excitation energy of the AS and 3 Å models of bR(BR) by 0.07 and 0.06 eV, respectively. The basis-sets' extension effect only by 0.01 eV the amount of the environmental QM effect. For the SAC-CI results, we used our previous data.[11,19,20] For the AS and RET models, calculations were performed at the SAC-CI/D95(d) level.[11,19,20] A frozen core approximation was adopted. A frozen virtual approximation was also adopted when the D95 and D95(d) basis sets[36] were used.

We are interested in excitation energies that take into account the environmental QM effect. The ONIOM scheme[37] was adopted for this purpose, and the SAC-CI excitation energy obtained using the AS model, $\Delta E^{\text{SAC-CI}}(\text{AS})$, was corrected using that obtained with the x Å model.

$$\Delta E(r_{\text{QM}} = x\text{Å}) = \Delta E^{\text{SAC-CI}}(\text{AS}) + [\Delta E^{\text{CIS}}(r_{\text{QM}} = x\text{Å}) - \Delta E^{\text{CIS}}(\text{AS})] \quad (1)$$

Hereafter, we refer to this computation scheme as SAC-CI:CIS/AMBER99.

Because the x value is the shortest distance between the chromophore and an environmental molecule, we introduced another index $\overline{r}_{\text{min}}$ that qualitatively represented the size of the QM region. This $\overline{r}_{\text{min}}$ index was an averaged value of r_{min} for each atom. The r_{min} was defined for each atom in the environment and was the shortest distance from the retinal chromophore.

2.2. MO Localization. Localized molecular orbitals (LMOs) were obtained using a scheme reported in our recent study.[29] We divided the protein model into many small fragments, which were classified into two categories. The first one includes amino acid residues (up to the C_α atom), water molecules, and ions, for which we prepared reference molecular orbitals (RMOs). Hartree–Fock canonical molecular orbitals (CMOs) were transformed into LMOs using the minimum orbital deformation (MOD) method[38] to maximize the overlap integrals with RMOs. The second one is the rest of the fragment, peptide bond units (–CO–NH–), and their MOs were localized using the Pipek–Mezey (PM) method.[39] Figure 2 shows an example of a model peptide. If we found a peptide bond, we placed borders at the C_α–C and C_α–N bonds. For fragments other than peptide bonds, we calculated RMOs and adopted MOD localization. To calculate the RMOs, a hydrogen atom was attached to the C_α atom as a link atom to compensate the valency. In the case illustrated by Figure 2, RMOs were calculated for fragments 1–4. Before the MOD localization, we performed singular value decomposition (SVD) to separate the orbital space for the RMOs from that for the peptide bonds. The orbital space for fragments 5 and 6 was obtained after SVD, and the PM method was performed for localization.

The result of the localization was analyzed, and the results for some typical systems are shown in Figure 3 for bR (BR state), Rh, and DPSB in MeOH. For each LMO, we calculated the Löwdin poplulation[40] on each fragment. To measure the extent of the localization, the maximum value of the population was obtained. Their distributions are summarized in Figure 3; about 75% of the LMOs in protein environments and 100% of those in a MeOH environment have more than 95% of the population within a single fragment. Approximately 95% of the LMOs have more than 80% of the population in a single fragment. In Figure S1 of the Supporting Information, we also show the overlap integrals between with LMOs and their corresponding RMO. Most of the overlap integrals exceed 0.85, which indicates that the present scheme localized the MO into a specific shape and into a specific region. In Figure S3 of the Supporting Information, we also show the distributions of MOs that have a fragment MO population less than 0.50 (the worst case). A total of 4 MOs fall under this criterion. Because they were all 2pσ-type orbitals of Gly, which have lobes in two neighboring amino acids, the MO population flowed into the neighbor fragment.

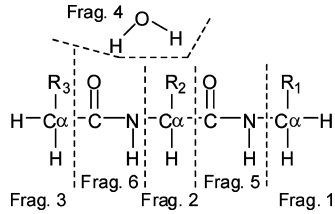

Figure 2. An example of the fragment borders used to calculate localized molecular orbitals.

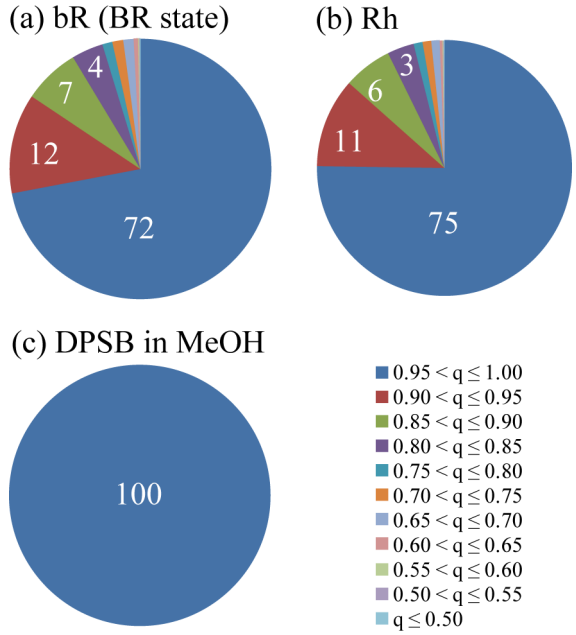

Figure 3. Result of Löwdin population analysis of the LMOs. Maximum population in a fragment, q, was calculated for each LMO. (a) bR (BR state, 6 Å model), (b) Rh (6 Å model), and (c) DPSB in MeOH environment (7 Å model). Number in the graph indicates the percentage.

QM/MM geometry optimization, MO localization, and LMO-CIS calculations were performed with the Gaussian program[41] modified for the present purposes.

3. RESULTS AND DISCUSSION

3.1. Extending the Wave Function to the Environment. First, we analyzed the environmental QM effects on the calculated excitation energy. Figure 4 shows the CIS/AMBER99 excitation energies of the retinal chromophore in HB, HG, HR, Rh, bR

dx.doi.org/10.1021/ct300510b | J. Chem. Theory Comput. 2012, 8, 4452–4461

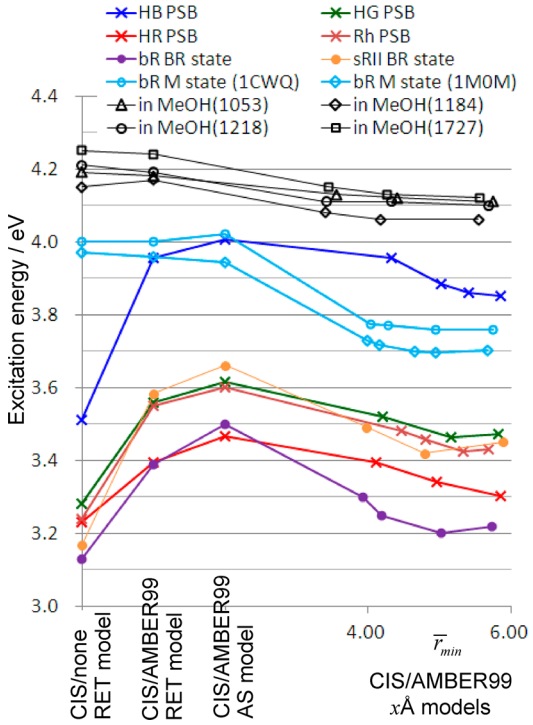

Figure 4. CIS/AMBER99 excitation energy of retinal chromophore in proteins and in methanol solution.

(BR state), bR (M state), sRII, and methanol solution. The size of the QM region was extended stepwise from the RET model first to the AS model and finally to the x Å model.

The "CIS/none QM region=RET" result represents the structural distortion effect on the calculated excitation energy. The calculated excitation energy of HB shown in Figure 4 was notably higher than the energies of the other three pigments. As reported in our previous study,[11,42] this difference is due to the C6−C7 twist in the retinal PSB in HB. The C6−C7 dihedral angle in HB was significantly larger than that in other cases. The "CIS/AMBER99 QM region=RET" results revealed an ES effect in the protein environment. Among the visual cone pigments, the calculated excitation energies of HB, Rh, HG, and HR increased by 0.45, 0.31, 0.28, and 0.16 eV, respectively, which clearly indicates that the ESP affected the relative excitation energy. These are the same conclusions obtained by our previous SAC-CI/MM study.[11] The excitation energy for bR (BR state) and sRII also increased by 0.26 and 0.41 eV, respectively. A larger ES contribution in sRII, which was reported in previous studies,[8,16,19,27] was also reproduced in the present calculations at the CIS/AMBER99 level. In contrast, the ES effect on the excitation energy of DPSB in bR (M state) and in methanol was negligibly small (−0.02 to +0.02 eV) because the ES interactions became weak due to the neutralization of both PSB and the counterion.[19] In addition, the intramolecular CT character of the excitation became small in DPSB.[19] The "CIS/AMBER99 QM region=AS" results reveal a quantum mechanical effect of the counterion. As shown in Figure 4, the calculated excitation energies increased when the point-charge model for the counterion was replaced with wave functions. However, the amounts by which the energies increased were 0.05−0.11 eV, which are similar in value. This result suggests that the QM effects of the counterion incorporated into these calculations are less important for the spectral shift among the retinal proteins. We arrived at a similar conclusion at the SAC-CI level of calculations.[11]

Next, we extended the wave function description to the environment. As shown in Figure 4, the calculated excitation energies decreased with the $\overline{r}_{min}$ value of the QM region and tended to converge at $\overline{r}_{min} \approx 6$ Å. The worst case was for HR: the excitation energy calculated with the 5 Å model ($\overline{r}_{min}$ = 4.96 eV) decreased by 0.03 eV as compared to the 6 Å model ($\overline{r}_{min}$ = 5.85 Å). As observed in Figure 4, the decreasing patterns are roughly classified into three cases. The first one, the mildest case, was observed in the result for MeOH solution. The calculated excitation energies obtained with the 3 Å model were already close to the convergence. The second case was observed for the visual pigments, Rh, HB, HG, and HR, which showed the second largest decrease in the excited state. The amount by which the energies decreased ranged from 0.17 to 0.14 eV. The observed similarity among the four is due to the similarity in the structures of these visual pigments, which have a common genetic origin. The third group, bR (both BR and M states) and sRII, showed the largest changes from the AS model. The amounts by which the energies decreased were 0.28, 0.26, and 0.21 eV in bR (BR state), bR (M state), and sRII, respectively. In a later section, the reason for this decrease will be described using the results of CIS/AMBER99 calculations with a LMO basis.

The results of the CIS calculations were used to correct the SAC-CI/MM excitation energies with the AS model. We adopted the ONIOM scheme as described in a previous section. The ONIOM-corrected excitation energies ("SAC-CI:CIS/AMBER99") are summarized in Table 1. The correction reduced

Table 1. Calculated Excitation Energies of Retinal Chromophores in Proteins and MeOH Solution

	calculated excitation energy (eV)			exptl.
system	SAC-CI/AMBER99 AS model	Δ^a	SAC-CI:CIS/AMBER99 (Dev.)^k	E_{abs} (eV)
HB	2.94^b	−0.16	2.78 (−0.21)	2.99^f
HG	2.32^b	−0.14	2.18 (−0.15)	2.33^g
HR	2.08^b	−0.16	1.92 (−0.28)	2.20^g
Rh	2.45^c	−0.17	2.28 (−0.21)	2.49^h
sRII	2.53^c	−0.21	2.32 (−0.17)	2.49^h
bR (BR)	2.23^c	−0.28	1.95 (−0.23)	2.18^i
bR (M)	3.10^d	−0.26	2.84 (−0.17)	3.01^j
MeOH	3.38^{d,e}	−0.10^e	3.28^e (−0.13)^e	3.41^j

^{a}CIS/AMBER99 correction using ONIOM scheme. ^{b}Reference 11. ^{c}Reference 19. ^{d}Reference 20. ^{e}Averaged values for four snapshots. ^{f}Reference 6. ^{g}Reference 7. ^{h}Reference 47. ^{i}Reference 48. ^{j}Reference 5. ^{k}Deviation from the experimental absorption energy.

the excitation energies by 0.10−0.28 eV. As a result, the SAC-CI:CIS/AMBER99 results underestimated the experimentally observed absorption energies by 0.13−0.28 eV. However, the relative excitation energies among the retinal proteins were actually improved. In Figure 5, the relative excitation energies obtained from the SAC-CI/AMBER99 and SAC-CI:CIS/AMBER99 calculations are compared to the experimental ones. The excitation energy of Rh was used as a reference. After the correction was taken into account, the deviation from the experiment in the relative excitation energy was improved to be +0.04, −0.02, and +0.04 eV for in sRII, bR(BR), and bR(M), respectively. The present correction has the right reason, which will be discussed in a later section. We note, however, that the correction was not sensitive to the relative excitation energies of the visual pigments. The agreement became even worse for the MeOH case. One possible reason is that the calculations in proteins included the counterions in AS model, while not in MeOH

dx.doi.org/10.1021/ct300510b | J. Chem. Theory Comput. 2012, 8, 4452−4461

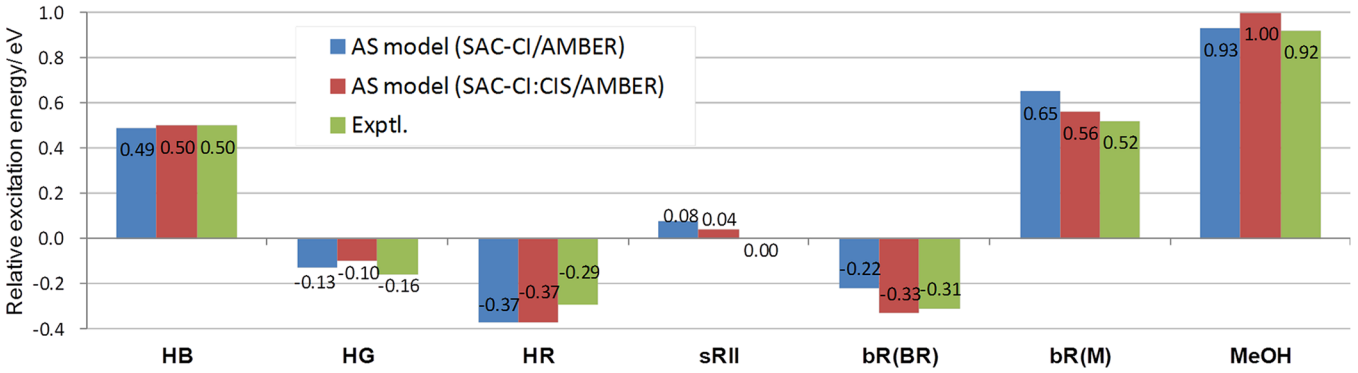

Figure 5. Relative excitation energies calculated with SAC-CI/AMBER99 and SAC-CI:CIS/AMBER99 were compared to experimental photoabsorption energy. The result for Rh was used as a reference.

solution, which could cause the definition of the environmental QM effect to become unbalanced between the protein and MeOH models.

To compare the CIS results with the DFT ones, we also adopted CAM-B3LYP calculations to describe the electronic effect of the protein environment. Because CT-type excitations could be involved in such large-scale calculations, we adopted a long-range corrected exchange-correlation functional.[43,44] In Figure 6, the CAM-B3LYP/AMBER99 results are compared to the CIS/AMBER99 results using the same model and basis sets. In each protein, the CAM-B3LYP/AMBER99 results were shifted such that the calculated excitation energy for the AS model is equal to that obtained with the CIS/AMBER99 result. As is clearly shown in Figure 6, the CAM-B3LYP calculations

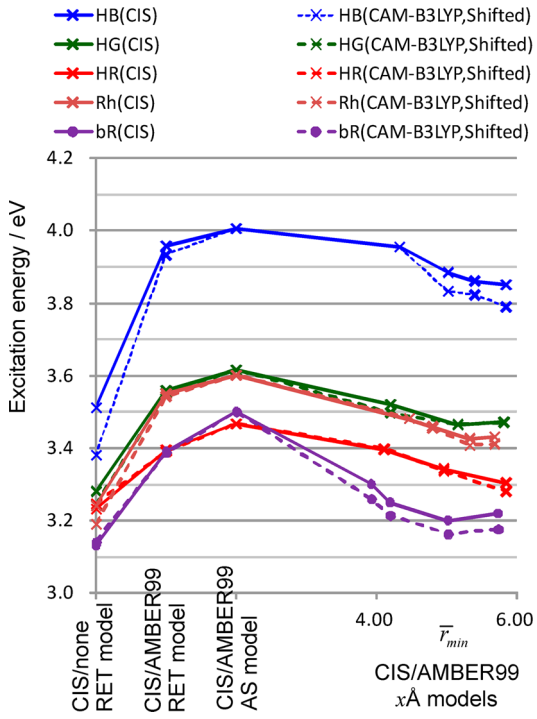

Figure 6. CIS/AMBER99 results were compared to CAM-B3LYP/AMBER99 results. CAM-B3LYP results for each protein were shifted, and the excitation energy obtained using the AS model is equal to that obtained by CIS/AMBER99.

produced results very similar to those provided by the CIS calculations. Starting from the AS model, the excitation energies decrease when the models with larger $\overline{r}_{min}$ values were adopted, and the CAM-B3LYP plots are very close to the CIS ones. The amount of the decrease at larger $\overline{r}_{min}$ values calculated with CAM-B3LYP tends to be larger than that with the CIS model. The largest deviation from the CIS result was, however, 0.06 eV in the 6 Å model for HB.

We also compared the DFT results to the experimental absorption energies. In the largest model (6 Å model), the calculated excitation energies obtained with the CAM-B3LYP/AMBER99 were 3.03, 2.74, 2.54, 2.70, and 2.51 eV for HB, HG, HR, Rh, and bR (BR state). The deviations from the experimental absorption energies were +0.04, +0.31, +0.34, +0.21, and +0.33 eV. The relative excitation energies were qualitatively reproduced, except for those of HB and Rh.

3.2. CIS Results Using Localized Molecular Orbitals.

Because the results indicate that the environmental effect, which was introduced by the CIS calculations, is not negligible, we must figure out what is the origin. However, if one adopts CMOs, the delocalized character of CMOs introduces ambiguity when interpreting the wave function. For example, we obtained CMOs for bR (BR state) using the 3 Å model as shown in Figure S4 in the Supporting Information. In the second main configuration, an excitation occurred in the MO delocalized toward the protein environment. Therefore, we performed CIS/AMBER99 calculations using MOs localized on each amino acid, water, and peptide bond. The results for bR (BR and M states) and Rh are summarized in Table 2.

The main configurations of the first excited state are HOMO-to-LUMO transitions of the retinal chromophore for all three cases: from MO 1746 to MO 5014 for the bR (BR state), from MO 1754 to MO 5048 for bR (M state), and from MO 1586 to MO 4501 for Rh, respectively. The distributions of these MOs are shown in Figure 7 and are clearly localized on the retinal moiety. The most important result is that an intermolecular CT excitation from Tyr185 to retinal chromophore becomes one of the main configurations for the cases of bR in BR and M states. MO 1491 in the BR state and MO 1499 in the M state are the HOMOs of Tyr185, which are clearly identified in the MO distributions shown in Figure 7. On the other hand, the main configurations of Rh do not involve a specific excited configuration relevant to the protein environment (see Figure S6 in the Supporting Information).

In section S3 of the Supporting Information, we also show lists of configurations that have a CI coefficient larger than 0.01. Many configurations related to the environment mix with the local excitation within the retinal chromophore. Tyr185 in bR makes large contributions as a CT donor and acceptor in addition to

dx.doi.org/10.1021/ct300510b | J. Chem. Theory Comput. 2012, 8, 4452−4461

Table 2. First Excited State of bR in the BR and M States and Rh Calculated Using LMOs[a]

	CIS[b]/AMBER99		SAC-CI/AMBER99		SAC-CI:CIS/AMBER99		exptl.	
	E_{ex}	main configurations ($\|Cl\| \geq 0.1$)[c]	E_{ex}	Δ	E_{ex}	Δ	E_{abs}	Δ
bR(BR)	3.22	+0.79(1746→5014) −0.41(1745→5014) +0.27(1746→5015) +0.14(**1491**→5014) −0.12(1744→5015) +0.12(1744→5014)	2.23[d]	(−0.22)	1.95	(−0.33)	2.18[g]	(−0.31)
bR(M)	3.76	+0.91(1754→5048) +0.25(1753→5049) +0.12(**1499**→5048) −0.11(1752→5050)	3.10[e]	(+0.65)	2.84	(+0.56)	3.01[f]	(+0.52)
Rh	3.43	+0.79(1586→4501) +0.42(1585→4501) −0.28(1586→4502) −0.19(1584→4501) −0.13(1584→4502)	2.45[d]	(0.00)	2.28	(0.00)	2.49[h]	(0.00)

[a]The MO indices in the environment are written in boldface. [b]The results of the 6 Å model were used. [c]Coefficients of spin-adapted configurations. For the MO distributions, see Figure 3 and Figure S1. [d]Reference 19. [e]Reference 20. [f]Reference 5. [g]Reference 48. [h]Reference 47.

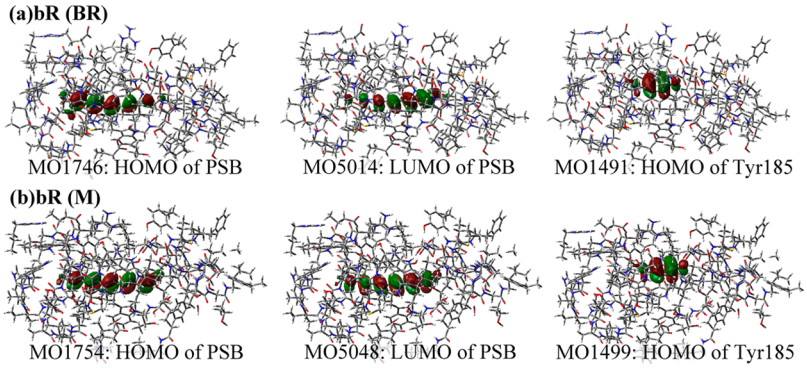

Figure 7. Distribution of MOs relevant to the first excited state of (a) bR (BR state) and (b) bR (M state). Isovalue of the MO surface was set to 0.02.

exciton coupling to the local excited state of the retinal chromophore.

3.3. A Course-Grained Analysis of the Excited-State Wave Function of the Protein Environment. In addition to the main configurations, we are also interested in other excitations in the environment that couple with excitations in the retinal chromophore. Because each MO is assigned to one of the fragments, the excited configurations $\{\phi_i^a\}$ are also classified into "groups" of excitations.

$$\Psi^{CIS} = \sum_{A}^{Frag}\sum_{i\in A}^{Occ}\sum_{B}^{Frag}\sum_{a\in B}^{Vac} d_i^a \phi_i^a = \sum_{A}^{Frag} \Phi_A^A + \sum_{A}^{Frag}\sum_{B\neq A}^{Frag} \Phi_A^B \quad (2)$$

d_i^a is the coefficient of the single excitation from MO i to MO a. A and B are fragment indices. The CI wave function is segmented into local excitations in each fragment $\{\Phi_A^A\}$ and CT excitations between two fragments $\{\Phi_A^B\}$ $(A \neq B)$. Hereafter, we call $\{\Phi_A^B\}$ an excitation group. To measure the contribution from each excitation group, the maximum value of $|d_i^a|$ in each excitation group was plotted for three typical systems, bR (BR state), Rh, and DPSB in MeOH solution, as shown in Figure 8 (subsequently identified as max$|d_{ai}|$ plot). It is very clearly illustrated that the excitations of the environment in bR (BR state) are more prominent than those in Rh and MeOH. In the next, the contribution of Tyr185 was observed in three types of excitations: local excitation, CT to PSB, and CT from PSB as shown in Figure 8a. Tyr185 in bR lies next to the retinal PSB, with the π planes of the two molecules parallel to each other, as shown in Figure 9. Local excitations in Trp86 also showed visible contributions, but the max$|d_{ai}|$ value was smaller than that in Tyr185. This is because the orientation of Trp86 with respect to PSB is different from that of Tyr185 (see Figure 9a). In the MeOH case shown in Figure 8b, we found that some CT excitations from the retinal chromophore to MeOH molecules have relatively large values. As shown in Figure 9, the MeOH molecules, which showed visible contributions, were located just above the π electron system of DPSB. The solvent molecules in these positions promote interactions with the π orbital of DPSB and contributed as CT-type excitations.

It is noteworthy that the distributions of the CI coefficients showed a characteristic localization, which indicates the structure of the excited-state wave function in proteins and solutions. As shown in Figure 8, the visible bars are primarily distributed on three lines. The first line is diagonal and is composed of local excitations in the fragments. The second line is an assembly of the CT excitations from the reference fragment, retinal chromophore. The third line is composed of the CT excitations toward the retinal chromophore. Therefore, these three lines are connected at the retinal→retinal excitation group. Considering this observation, the effective representation of the excited-state wave function would be:

$$\Psi^{CIS,Total} = \Phi^{Ref} + \sum_{X}^{Frag} \Phi^{Ref\to X} + \sum_{X}^{Frag} \Phi^{X\to Ref} + \sum_{X}^{Frag} \Phi^{X\to X} \quad (3)$$

The first term in eq 3 is local excitations of the reference fragment (ref), retinal chromophore. The second and third terms are CT from and to ref, respectively. The fourth term represents local excitations in each fragment. This is a reasonable expression because the three types of excitations (the second, third, and fourth terms in eq 3) are involved in the first-order interacting space with respect to the reference-state wave function (the first term in eq 3) that is described with singly excited configurations. CT excitations between the amino acids residues have very small coefficients in the wave function because these CT excitations lie

dx.doi.org/10.1021/ct300510b | J. Chem. Theory Comput. 2012, 8, 4452−4461

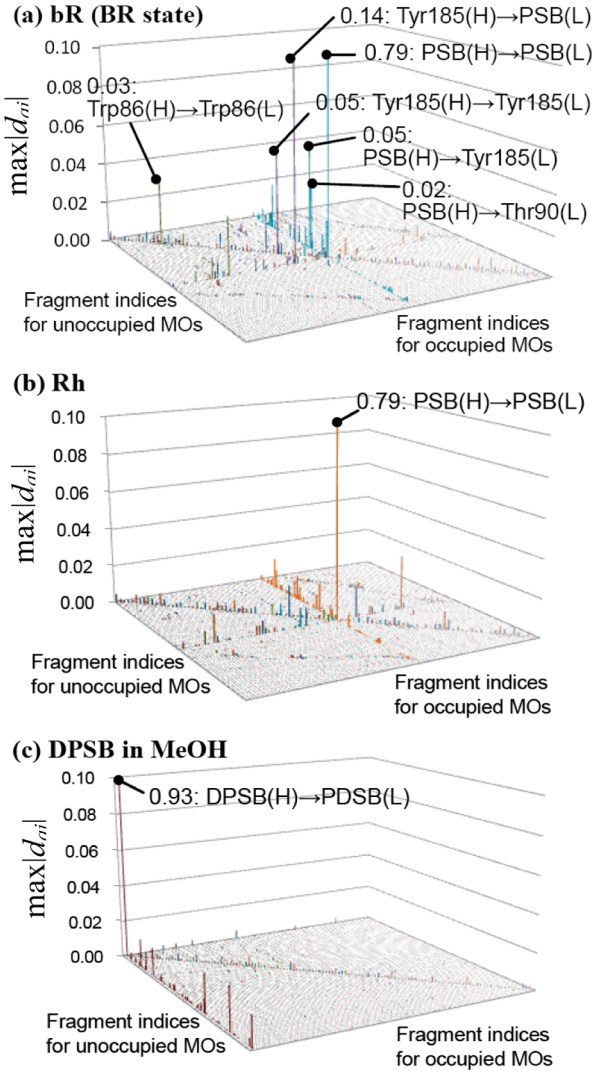

Figure 8. Max$|d_{ai}|$ plot for the first excited state of (a) bR (BR state), (b) Rh, and (c) DPSB in MeOH.

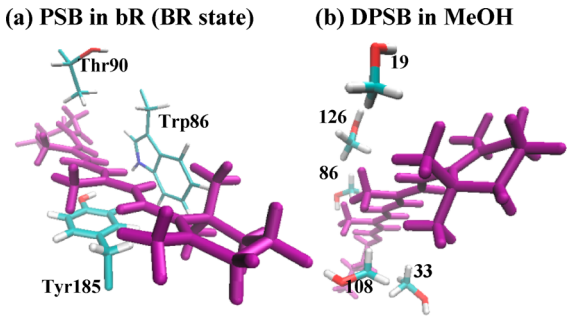

Figure 9. Molecular fragments participating in the excited states of the retinal chromophore. (a) PSB and some amino acid residues in bR (BR state). (b) DPSB and some methanol molecules in the MeOH solution.

outside of the first-order interaction space. Figure 8 a and b shows lines of minor plots in the off-diagonal part of the diagram. These plots are derived from CT excitations between amino acid residues and their adjacent peptide bond fragment. As described in section 2.2 and the Supporting Information, because some of the LMOs have "tails" on adjacent fragments, the CT excitations of this kind involve a local excitation character, which comes into the first-order interaction space in the wave function.

We are also interested in how excitations in each fragment depend on the distance from the retinal chromophore. To measure the contributions from each fragment to the wave function, we introduced the norm of an excitation group as follows:

$$N_{A,B} = \sqrt{\sum_{i\in A}^{\mathrm{Occ}} \sum_{a\in B}^{\mathrm{Vac}} |d_i^a|^2} \qquad (4)$$

The summation of the orbital indices, i and a, runs within the fragments A and B, respectively. The positions of the fragments were defined by the $\overline{r}_{\mathrm{min}}$ value for each fragment (see the Computational Details for definition). For a fragment at the $\overline{r}_{\mathrm{min}}$ distance, we evaluated the norms for CTs to retinal, CTs from retinal, and local excitations in the fragment. In Figure 10, the

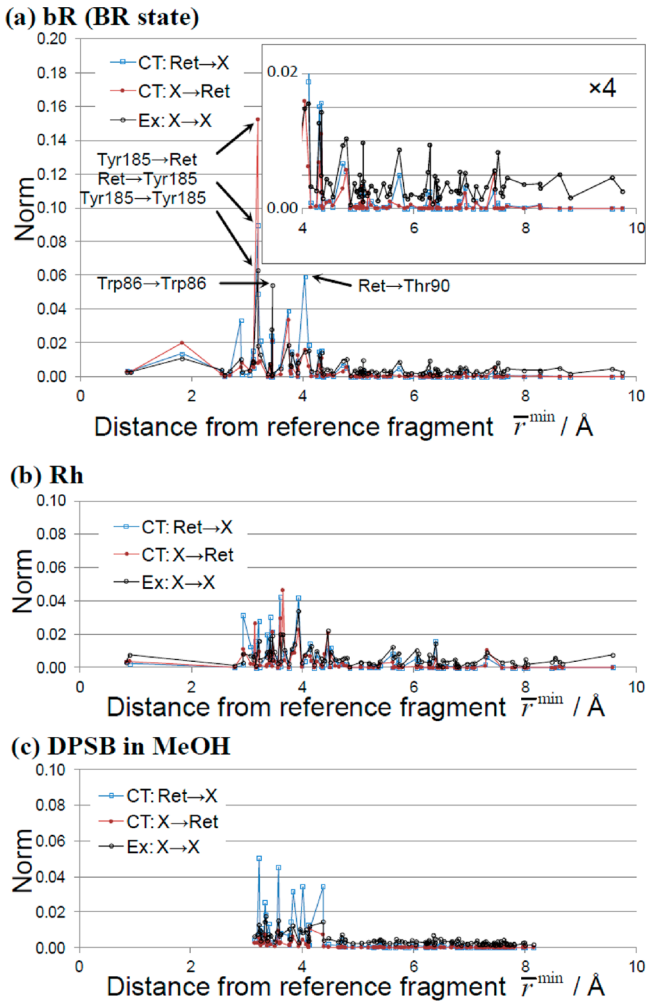

Figure 10. Fragment norm versus $\overline{r}^{\mathrm{min}}$ (see text for definition). CIS wave functions for the first excited state of (a) bR (BR state), (b) Rh, and (c) DPSB in MeOH (a snapshot). "X" denotes a fragment in the protein environment.

results for bR (BR state), Rh, and MeOH solutions are compared. For the case of MeOH solution, other snapshot structures also showed similar diagrams, which are presented in Figure S4. As shown in Figure 10a, the plot for bR shows large spikes within $\overline{r}_{\mathrm{min}}$= 4 Å from the retinal chromophore. The $N_{A,B}$ values of bR were relatively larger than those observed in Rh and MeOH solution. This trend is consistent with the result of the

dx.doi.org/10.1021/ct300510b | J. Chem. Theory Comput. 2012, 8, 4452−4461

max|d_{ai}| plot shown in Figure 8. Among the three figures, we clearly found that the CT contributions decay rapidly with the distance from the chromophore because a CT excitation between the retinal chromophore and an environmental fragment is essentially equivalent to an orbital interaction that decays exponentially with the distance between the donor and acceptor. The appearance of the CT spikes is limited to within the $\overline{r}_{min}$ = 4 Å region. This region corresponds to the so-called first solvation layer (FSL). The local excitations became dominant in longer-$\overline{r}_{min}$ regions. This result is commonly observed in the three cases. This relatively slower decay with the $\overline{r}_{min}$ distance could be related to the decay behavior of the exciton−exciton coupling that shows a polynomial decay with distance. In Figure S4 of the Supporting Information, we also show an additional three diagrams for DPSB in MeOH solution. These diagrams similarly show the contribution of methanol molecules in FSL. However, there is no common spike in the four diagrams in the MeOH cases. Because the interactions between DPSB and methanol solvent are weak, there is no fixed configuration for the solvent molecules.

To summarize this section, additional information is included regarding the structure of the wave function.

$$\Psi^{\mathrm{CIS,Total}} = \Phi^{\mathrm{Ref}} + \sum_{X\in\mathrm{FSL}}^{\mathrm{Frag}} \Phi^{\mathrm{Ref}\rightarrow X} + \sum_{X\in\mathrm{FSL}}^{\mathrm{Frag}} \Phi^{X\rightarrow \mathrm{Ref}} + \sum_{X}^{\mathrm{Frag}} \Phi^{X\rightarrow X} \tag{5}$$

Here, the CT excitations are restricted to fragments in the first solvation layer. This expression would be useful when taking into account the solvation effect in calculating the excited states of molecules in proteins and solutions.

3.4. Excitation-Energy Decomposition Analysis. Before closing this section, we explain the contribution to the excitation energy. Here, we analyzed the contributions of each fragment as follows:

$$E_{\mathrm{ex}}^{\mathrm{Tot}} = E_{\mathrm{LEx}}^{\mathrm{Ref}} + \sum_{A\neq\mathrm{Ref}}^{\mathrm{Frag}} E_{\mathrm{LEx}}^{A} + \sum_{A\neq\mathrm{Ref}}^{\mathrm{Frag}} E_{A\rightarrow\mathrm{Ref}}^{A} + \sum_{A\neq\mathrm{Ref}}^{\mathrm{Frag}} E_{\mathrm{Ref}\rightarrow A}^{A} + (\mathrm{others}) \tag{6}$$

Excitation energy of the total system was decomposed into the reference fragment, $E_{\mathrm{LEx}}^{\mathrm{Ref}}$, local excitations (LEx) in a fragment A, E_{LEx}^{A}, CT from a fragment A to the reference fragment, $E_{A\rightarrow\mathrm{Ref}}^{A}$, CT from the reference fragment to a fragment A, $E_{\mathrm{Ref}\rightarrow A}^{A}$, and the others. The $E_{\mathrm{LEx}}^{\mathrm{Ref}}$ term was defined as

$$E_{\mathrm{ex}}^{\mathrm{Ref}} = \langle 0|\hat{H}|0\rangle,\ |0\rangle \equiv \sum_{ia\in\mathrm{Ref}}^{\mathrm{MO}} |_i^a\rangle d_i^a \tag{7}$$

$\{d_i^a\}$ were the CIS coefficients calculated for the total system. The other three terms, E_{LEx}^{A}, $E_{A\rightarrow\mathrm{Ref}}^{A}$, and $E_{\mathrm{Ref}\rightarrow A}^{A}$, were defined as

$$E_X^A = \langle X|\hat{H}|X\rangle + 2^*\langle 0|\hat{H}|X\rangle \tag{8}$$

X was classified into LEx, $A\rightarrow$Ref, and Ref$\rightarrow A$, and defined as $|\mathrm{LEx}\rangle \equiv \sum_{ia\in A}^{\mathrm{MO}} |_i^a\rangle d_i^a$, $|A\rightarrow\mathrm{Ref}\rangle \equiv \sum_{i\in A}^{\mathrm{MO}}\sum_{i\in\mathrm{Ref}}^{\mathrm{MO}} |_i^a\rangle d_i^a$, and $|\mathrm{Ref}\rightarrow A\rangle \equiv \sum_{i\in\mathrm{Ref}}^{\mathrm{MO}}\sum_{i\in A}^{\mathrm{MO}} |_i^a\rangle d_i^a$, respectively. Table 3 shows the result for the first excited state of bR (BR state, 6 Å model), which has the largest contribution from the environmental fragments among the systems investigated in the present study. Calculated excitation energy for this model was 3.22 eV. Because the excitation in the reference fragment, retinal chromophore, was 3.58 eV, the environmental excitations reduce excitation energy by 0.36 eV. The most prominent reduction (−0.24 eV) arises from CT to the reference fragment, retinal PSB. The secondary reduction (−0.07 eV) is from the local excitation in the environmental fragments. We also investigated the specific contributors and found that CT from Tyr185 to RET contributes by −0.10 eV, which agrees with the conclusion derived from the analysis of the excited-state wave function.

Table 3. Excitation Energy of bR(BR) with 6 Å Model Was Decomposed into Contributions from the Group Excitations[a]

excitation	E^X
total	3.22
RET → RET	3.58
X → X	−0.07
RET → X	+0.02
X → RET	−0.24
other terms	−0.06
large contributions	
Tyr185 → RET	−0.10
Thr90 → RET	−0.04
RET → Tyr185	+0.03
Met118→ RET	−0.02
Pro186 → RET	−0.02
Trp86 → Trp86	−0.01
Ala215 → RET	−0.01

[a]Units are in electronvolts.

4. CONCLUSIONS

In our previous study,[20] we indicated that the QM treatment for the environment gave a non-negligible change in calculated excitation energy of DPSB in a protein environment and in MeOH solution. In this study, we performed CIS calculations with a particular focus on polarization and charge transfer effects of the environment and extended our investigation to HB, HG, HR, Rh, bR, and sRII. We found that the environmental contribution described quantum mechanically by the CIS calculations is commonly important in the calculated excitation energy among all of the systems. The calculated excitation energies were reduced by 0.1−0.3 eV, as compared to the MM description for the environmental effect. The CIS results were combined with the SAC-CI one using the ONIOM scheme, and the CIS correction for the environmental effect also helped to improve the accuracy of the relative excitation energies.

To understand the origin of the environmental effect included by the CIS calculations, we introduced a LMO picture into the excited-CI wave function. Our LMO transformation scheme works well for the retinal proteins and MeOH solution, and delocalized CMOs were localized within predefined regions and shapes. From an LMO point of view, we could identify the specific roles of amino acids in the environmental CI wave function. In bR, where the CIS gave the largest change, Tyr185 was involved in CT excitation to retinal, CT from retinal, and a local exciton within Tyr185. In addition, many CTs and exciton contributions were found in the CI wave function. The results were corroborated by an excitation-energy decomposition analysis. However, we also note that the CIS correction improves the ESP of the environment and introduced a part of the change in the calculated excitation energy.

We also analyzed the structure of the environmental CI wave functions. We found that the CI wave functions have a specific structure common to all retinal proteins and MeOH solution. The CI coefficients distribute primarily in the CT from retinal, CT to retinal, and local excitations within each fragment. We also investigated the radial distribution of the CI coefficients. The results clearly revealed particular CT contributions of the amino

acids in the FSL. The CT contribution decayed rapidly with the distance from retinal, and local excitations produced larger contributions in longer distances. These results indicated the response of the protein environment when the excitation occurred in the retinal chromophore. At the same time, the results of the analysis indicated the structure of the environmental CI wave function. In a future study, it would also be interesting to investigate the quantitative accuracy of the structure of the wave function described by eqs 3 and 5. Although the polarizable continuum model works successfully to describe the electrostatic interactions in solution,[45,46] there is no established computational model for the protein environment. The present results may help to build a new computational model for describing the environmental effect in solvatochromism.

■ ASSOCIATED CONTENT

Supporting Information

Some properties of LMOs. Norm versus $\bar{r}^{min}$ distance plot for DPSB in MeOH solution. Excited configurations for bR (BR state) calculated with 6 Å model. CMOs obtained for bR (BR state) using 3 Å model. LMOs in Rh. Basis-sets extension effect on calculated excitation energy. This material is available free of charge via the Internet at http://pubs.acs.org.

■ AUTHOR INFORMATION

Corresponding Author

*E-mail: hasegawa@cat.hokudai.ac.jp.

Present Address

[⊥]Catalysis Research Center, Hokkaido University, Kita21, Nishi10, Kita-ku, Sapporo, Hokkaido, Japan, 001-0021.

Notes

The authors declare no competing financial interest.

■ ACKNOWLEDGMENTS

This study was supported by KAKENHI (21685002, 24350008) from the Japan Society for the Promotion of Science (JSPS), JST-CREST, and Strategic Programs for Innovative Research (SPIRE). K.J.F. appreciates KAKENHI (23108709). A portion of the computations was carried out at RCCS (Okazaki, Japan) and ACCMS (Kyoto University).

■ REFERENCES

(1) Reichardt, C. *Chem. Rev.* **1994**, *94*, 2319−2358.
(2) Lozier, R. H.; Bogomolni, R. A.; Stoeckenius, W. *Biophys. J.* **1975**, *15*, 955−962.
(3) Oesterhelt, D.; Stoeckenius, W. *Proc. Natl. Acad. Sci. U.S.A.* **1973**, *70*, 2853−2857.
(4) Nakanishi, K.; Baloghnair, V.; Arnaboldi, M.; Tsujimoto, K.; Honig, B. *J. Am. Chem. Soc.* **1980**, *102*, 7945−7947.
(5) Gat, Y.; Sheves, M. *Photochem. Photobiol.* **1994**, *59*, 371−378.
(6) Fasick, J. I.; Lee, N.; Oprian, D. D. *Biochemistry* **1999**, *38*, 11593−11596.
(7) Asenjo, A. B.; Rim, J.; Oprian, D. D. *Neuron* **1994**, *12*, 1131−1138.
(8) Hayashi, S.; Tajkhorshid, E.; Pebay-Peyroula, E.; Royant, A.; Landau, E. M.; Navarro, J.; Schulten, K. *J. Phys. Chem. B* **2001**, *105*, 10124.
(9) Vreven, T.; Morokuma, K. *Theor. Chem. Acc.* **2003**, *109*, 125.
(10) Coto, P. B.; Strambi, A.; Ferré, N.; Olicucci, M. *Proc. Natl. Acad. Sci. U.S.A.* **2006**, *103*, 17154−17159.
(11) Fujimoto, K.; Hasegawa, J.; Nakatsuji, H. *Bull. Chem. Soc. Jpn.* **2009**, *82*, 1140−1148.
(12) Hasegawa, J.; Fujimoto, K.; Nakatsuji, H. *ChemPhysChem* **2011**, *12*, 3106−3115.
(13) Sekharan, S.; Katayama, K.; Kandori, H.; Morokuma, K. *J. Am. Chem. Soc.* **2012**, *134*, 10706−10712.
(14) Ryazantsev, M. N.; Altun, A.; Morokuma, K. *J. Am. Chem. Soc.* **2012**, *134*, 5520−5523.
(15) Tomasello, G.; Olaso-González, G.; Altoè, P.; Stenta, M.; Serrano-Andrés, L.; Merchán, M.; Orlandi, G.; Bottoni, A.; Garavelli, M. *J. Am. Chem. Soc.* **2009**, *131*, 5172−5186.
(16) Wanko, M.; Hoffmann, M.; Frauenheim, T.; Elstner, M. *J. Phys. Chem. B* **2008**, *112*, 11462−11467.
(17) Warshel, A.; Levitt, M. *J. Mol. Biol.* **1976**, *103*, 227−249.
(18) Wang, J.; Cieplak, P.; Kollman, P. A. *J. Comput. Chem.* **2000**, *21*, 1049−1074.
(19) Fujimoto, K.; Hayashi, S.; Hasegawa, J.; Nakatsuji, H. *J. Chem. Theory Comput.* **2007**, *3*, 605−618.
(20) Fujimoto, K.; Asai, K.; Hasegawa, J. *Phys. Chem. Chem. Phys.* **2010**, *12*, 13107−13116.
(21) Hasegawa, J.; Ise, T.; Fujimoto, K.; Kikuchi, A.; Fukumura, E.; Miyawaki, A.; Shiro, Y. *J. Phys. Chem. B* **2010**, *114*, 2971−2979.
(22) Houjou, H.; Inoue, Y.; Sakurai, M. *J. Phys. Chem. B* **2001**, *105*, 867−879.
(23) Sakurai, M.; Sakata, K.; Saito, S.; Nakajima, S.; Inoue, Y. *J. Am. Chem. Soc.* **2003**, *125*, 3108−3112.
(24) Wesolowski, T. A. *J. Am. Chem. Soc.* **2004**, *126*, 11444−11445.
(25) Neugebauer, J. *J. Phys. Chem. B* **2008**, *112*, 2207−2217.
(26) Wanko, M.; Hoffmann, M.; Frähmcke, J.; Frauenheim, T.; Elstner, M. *J. Phys. Chem. B* **2008**, *112*, 11468−11478.
(27) Ren, L.; Martin, C. H.; Wise, K. J.; Gillespie, N. B.; Luecke, H.; Lanyi, J. K.; Spudich, J. L.; Birge, R. R. *Biochemistry* **2001**, *40*, 13906.
(28) Kaila, V. R.; Send, R.; Sundholm, D. *J. Phys. Chem. B* **2012**, *116*, 2249−2258.
(29) Hasegawa, J.; Kawatsu, T.; Toyoya, K.; Matsuda, K. *Chem. Phys. Lett.* **2011**, *508*, 171−176.
(30) Hayashi, S.; Ohmine, I. *J. Phys. Chem. B* **2000**, *104*, 10678.
(31) Case, D. A.; Darden, T. A.; Cheatham, I.; Simmerling, C. L.; Wang, J.; Duke, R. E.; Luo, R.; Crowley, M.; C.Walker, R.; Zhang, W.; Merz, K. M.; Wang, B.; Hayik, S.; Roitberg, A.; Seabra, G.; Kolossváry, I.; Wong, K. F.; Paesani, F.; Vanicek, J.; Wu, X.; Brozell, S. R.; Steinbrecher, T.; Gohlke, H.; Yang, L.; Tan, C.; Mongan, J.; Hornak, V.; Cui, G.; Mathews, D. H.; Seetin, M. G.; Sagui, C.; Babin, V.; Kollman, P. A. *AMBER 10*; University of California: San Francisco, CA, 2008.
(32) Stenkamp, R. E.; Filipek, S.; Driessen, C. A. G. G.; Teller, D. C.; Palczewski, K. *Biochim. Biophys. Acta* **2002**, *1565*, 168.
(33) Ferré, N.; Cembran, A.; Garavelli, M.; Olivucci, M. *Theor. Chem. Acc.* **2004**, *112*, 335−341.
(34) Hehre, W. J.; Ditchfield, R.; Pople, J. A. *J. Chem. Phys.* **1972**, *56*, 2257.
(35) Hariharan, P. C.; Pople, J. A. *Theor. Chim. Acta* **1973**, *28*, 213.
(36) Dunning, T. H.; Hay, P. J. In *Methods of Electronic Structure Theory, III*; Schaefer, H. F., Ed.; Plenum Press: New York, 1977.
(37) Maseras, F.; Morokuma, K. *J. Comput. Chem.* **1995**, *16*, 1170.
(38) Toyota, K.; Ehara, M.; Nakatsuji, H. *Chem. Phys. Lett.* **2002**, *356*, 1−6.
(39) Pipek, J.; Mezey, P. G. *J. Chem. Phys.* **1989**, *90*, 4916−4926.
(40) Löwdin, P. O. *Adv. Quantum Chem.* **1970**, *5*, 185−200.
(41) Frisch, M. J.; Trucks, G. W.; Schlegel, H. B.; Scuseria, G. E.; Robb, M. A.; Cheeseman, J. R.; Montgomery, J. A.; Vreven, T.; Kudin, K. N.; Burant, J. C.; Millam, J. M.; Iyengar, S. S.; Tomasi, J.; Barone, V.; Mennucci, B.; Cossi, M.; Scalmani, G.; Rega, N.; Petersson, G. A.; Nakatsuji, H.; Hada, M.; Ehara, M.; Toyota, K.; Fukuda, R.; Hasegawa, J.; Ishida, M.; Nakajima, T.; Honda, Y.; Kitao, O.; Nakai, H.; Klene, M.; Li, X.; Knox, J. E.; Hratchian, H. P.; Cross, J. B.; Adamo, C.; Jaramillo, J.; Gomperts, R.; Stratmann, R. E.; Yazyev, O.; Cammi, R.; Pomelli, C.; Ochterski, J.; Ayala, P. Y.; Morokuma, K.; Hase, W. L.; Voth, G.; Salvador, P.; Dannenberg, J. J.; Zakrzewski, V. G.; Dapprich, S.; Daniels, A. D.; Strain, M. C.; Farkas, O.; Malick, D. K.; Rabuck, A. D.; Raghavachari, K.; Foresman, J. B.; Ortiz, J. V.; Cui, Q.; Baboul, A. G.; Clifford, S.; Cioslowski, J.; Stefanov, B. B.; Liu, G.; Liashenko, A.; Piskorz, P.; Komaromi, I.; Martin, R. L.; Fox, D. J.; Keith, T.; Al-Laham, M. A.; Peng, C. Y.; Nanayakkara, A.; Challacombe, M.; Gill, P. M. W.;

Johnson, B.; Chen, W.; Wong, M. W.; Gonzalez, C.; Pople, J. A. *Gaussian Development Version*, revision A.03; Gaussian, Inc.: Pittsburgh, PA, 2003.
(42) Fujimoto, K.; Hasegawa, J.; Hayashi, S.; Nakatsuji, H. *Chem. Phys. Lett.* **2006**, *423*, 252−256.
(43) Tawada, Y.; Tsuneda, T.; Yanagisawa, S.; Yanai, T.; Hirao, K. *J. Chem. Phys.* **2004**, *120*, 8425−8433.
(44) Yanai, T.; Tew, D.; Handy, N. *Chem. Phys. Lett.* **2004**, *893*, 51−57.
(45) Tomasi, J.; Mennucci, B.; Cammi, R. *Chem. Rev.* **2005**, *105*, 2999−3093.
(46) Cammi, R.; Fukuda, R.; Ehara, M.; Nakatsuji, H. *J. Chem. Phys.* **2010**, *133*, 024104.
(47) Kandori, H.; Schichida, Y.; Yoshisawa, T. *Biochemistry (Moscow)* **2001**, *66*, 1197−1209.
(48) Birge, R. R.; Zhang, C. F. *J. Chem. Phys.* **1990**, *92*, 7178−7195.